Analytical Model and Design of 4H-SiC Planar and Trenched JBS Diodes

Luigi Di Benedetto, *Member, IEEE*, Gian Domenico Licciardo, *Member, IEEE*, Tobias Erlbacher, Anton J. Bauer, and Salvatore Bellone, *Member, IEEE*

***Abstract*— An analytical instrument to design 4H-SiC planar and trenched Junction Barrier Schottky diodes is proposed. The tool is based on a novel full analytical description of the electric field distribution into channel region of the device under reverse bias conditions. The model favorably exploits compact and reversible expressions that take into account all physical and geometrical quantities of the device in order to calculate the electric field at the Schottky contact as well as the reverse diode current, up to the occurrence of the physical limits of the Schottky junction. Differently than the existent literature, the generality of the model is achieved by the absence of empirical parameters, since all the expressions are analytically derived. An algorithm is finally reported to illustrate the design capability of the model for a generic JBS structure having planar, trenched or recessed p-type regions. Comparisons with numerical simulations and experimental data are presented to validate the model.**

***Index Terms*—4H−SiC Junction Barrier Schottky diodes, Design methodology, Schottky barrier, Semiconductor device modeling, Silicon compound.**

I. Introduction

FOR medium and high-power applications, 4H-SiC Junction Barrier Schottky (JBS) diodes have met a good commercial success that continues to stimulate their technological and topological improvements [1]−[6]. Nowadays, both planar (Fig.1.a) [7] and trenched (Fig.1.b) [4] JBS (TJBS) structures have been demonstrated, which combine lower forward voltage drop than 4H-SiC $p-i-n$ diodes and blocking voltages, V_{BL}, in the range of $1kV$ and $10kV$ [7]−[9], allowed by the shielding effect of p^+−type implanted regions. Indeed, when a reverse bias voltage, V_D, is applied, it almost entirely drops across the horizontal $p-n$ junctions shielding the Schottky contact and the diode reverse current, J_D, can be substantially reduced being directly dependent on Schottky electric field, E_{SCH}.

Therefore, the aim of designing both JBS topologies is to optimize the channel region, which is the epilayer portion circumscribed by p^+−regions and the Schottky contact as shown in Fig.1. Such design can be efficiently initiated by a convenient analytical model that allows one to calculate an initial set of geometrical quantities satisfying all electrical specifications. A look at the recent literature reveals that, although various models for 4H-SiC JBS in reverse bias conditions have been proposed [10]−[12], they are not adequate to be used as general design instruments of JBS structures due to their implicit assumptions or to their expressions. In particular,

- E_{SCH}−dependency on channel geometry is defined by using fitting parameters obtained after comparisons with either experimental data or numerical simulations [10];
- the introduction of empirical or semi-empirical expressions obtained from linear fit among model and numerical simulations [11], that reduces the applicability of the model;
- the use of not reversible expressions that make impossible a straightforward calculation of the channel geometries in terms of the maximum Schottky electric field [11]−[12].

In this paper, with the aim to give a straightforward design methodology for JBS diodes, we propose a novel analytical model of E_{SCH}, which works with different geometries. Strength−points of the proposed model are:

- compactness of the derived equations, that, being all in closed-form, can be easily inverted in order to make explicit the most relevant relationships between E_{SCH} and physical and geometrical parameters of the devices;
- absence of empirical fitting coefficients, which makes straightforward and sufficiently general its application in the designing of planar and trenched JBS diodes;
- a more general channel geometry having considered also buried p^+−regions.

The paper is organized as follows: in Section II the introduction to our design methodology is reported; in Section III the analytical model is shown and in Section IV its validity is verified by comparisons with numerical simulation results and experimental measurements; in Section V the design tool, developed by the model, is proposed. Section VI concludes the paper.

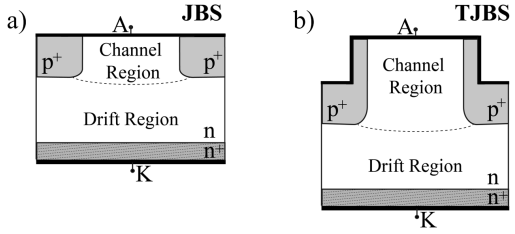

Fig. 1. a) Planar and b) trenched JBS diodes cross-section views.

This work was supported in part by the Ministero dell'Istruzione, dell'Università e della Ricerca under Grant PON03PE_00159_1(Project NEMBO). L. Di Benedetto, G.D. Licciardo and S. Bellone are with the Department of Industrial Engineering, University of Salerno, Italy. (e-mail: ldibenedetto@unisa.it, gdlicciardo@unisa.it, sbellone@unisa.it).

T. Erlbacher and A.J. Bauer are with the Fraunhofer Institute for Integrated Systems and Device Technology (IISB), Erlangen, Germany. (e-mail:tobias.erlbacher@iisb.fraunhofer.de, anton.bauer@iisb.fraunhofer.de).

II. Structure and Design of JBS Devices

In our model we consider the JBS structure of Fig.2.a having p^+−regions far Y_R from the Schottky junction so that a planar or trench JBS (see Fig.1) is given for Y_R=0μm whereas a JBS with recessed p^+−regions has Y_R>0μm. The other parameters are the distance among p^+−regions, X_{CH}, their depth, Y_G, and width, X_G, and the epilayer thickness, Y_{EPI}, and doping concentration, N_{EPI}. It is worth to note that in all cases p^+−regions and the Schottky contact are short-circuited.

The electrical behavior of a JBS diode is identified by the on-state total resistance, R_D, for forward operation and the blocking voltage, V_{BL}, for reverse biasing. R_D can be expressed as follows [10]−[12]:

$$R_D = R_{CH} + R_{SP} + R_{EPI} + R_{SUB} + R_{CONT} \qquad (1)$$

where

$R_{SP} = (X_{CH} + X_G)0.5\rho_{EPI} \ln\left[(X_{CH} + X_G)/(X_{CH} - 2W_{SC})\right]$ is the spreading resistance, $R_{EPI} = \rho_{EPI}(Y_{EPI} - 0.5X_G)$ the drift resistance, $R_{SUB} = \rho_{SUB}Y_{SUB}$ the substrate resistance, $R_{CH} = \rho_{EPI}Y_{CH}(X_{CH} + X_G)(X_{CH} - 2W_{SC})^{-1}$ is the channel resistance, R_{CONT} the contact resistance [13], W_{SC} p−n space charge region in forward condition and, finally, $\rho_{EPI(SUB)}$ the epilayer (substrate) resistivity.

It is known that when a reverse biased 4H-SiC Schottky contact is exposed to high electric fields, it manifests a significant increase of the leakage current due to the electron tunneling through the Schottky barrier [14]. To limit the tunneling current, the electric field at the Schottky junction, E_{SCH}, must be kept low so that the thermionic current, I_{TE}, is higher than the field emission one, I_{FE}. In the following discussion, we impose I_{TE}/I_{FE}=100, in order to limit E_{SCH} to about $1MVcm^{-1}$ [10]-[12], and, consequently, we define as blocking voltage, V_{BL}, the reverse voltage value that gives such electric field. It is important to note that both, R_D and V_{BL}, are defined by X_{CH} and $Y_{CH}=Y_G+Y_R$ [10]-[12].

However, while (1) can be directly used to meet constrains on R_D, a full analytical and reversible equation in terms of geometrical quantities of E_{SCH} has not been proposed in the literature up to now. Therefore, the following section will concentrate on the solution of this challenge.

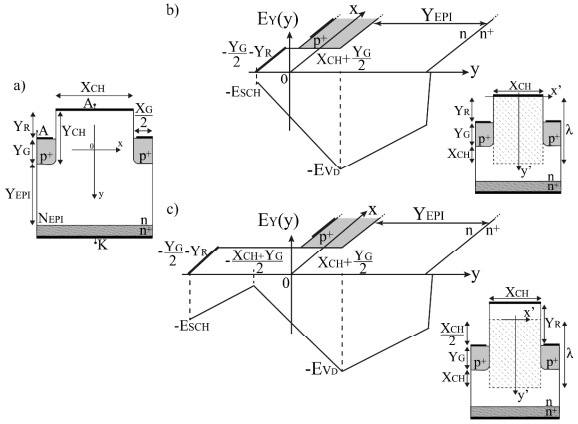

Fig. 2. a) Cross-section view of a general JBS structure with the main physical and geometrical parameters. Cutaway of $E_Y(0,y)$ and model domain regions for JBS diode with b) $Y_R \leq X_{CH}/2$ and c) $Y_R > X_{CH}/2$.

III. Model of Schottky Electric Field

Similarly to Vertical-JFET (VJFET)−based structures [15]−[16], under high reverse voltages, p^+−n space charge regions overlap into the channel region. The interactions of electric fields at p^+−n junction corners extends up to $(x,y)=(0,X_{CH}+Y_G/2)$ where the E_Y−distribution changes the slope, as schematized in Fig.1.b and c, and occupies an area depth, λ, and width, X_{CH}. After this point, the electric field vertically extends in the drift region with a slope of qN_{EPI}/ε towards the substrate. The minimum value of E_Y at $(x,y)=(0,X_{CH}+Y_G/2)$ is equal to [16]:

$$E_{V_D} = E_{pn} - q\frac{N_{EPI}}{\varepsilon}X_{CH} \qquad (2)$$

where

$$E_{pn} = q\frac{N_{EPI}}{\varepsilon}Y_{EPI} + \frac{V_D - V_{PT}}{Y_{EPI}} \qquad (3)$$

is the electric field at junction edge having assumed that p−i−n has reached the punch−through condition, $V_{PT} = qN_{EPI}/(2\varepsilon)Y_{EPI}^2 - V_{bi}^{pn}$ is the punch−through voltage, $V_{bi}^{pn} = V_T \ln\left(N_{EPI}N_A^-/n_i^2\right)$ the p^+−n built−in voltage, N_A^- the p^+−region ionized doping concentration and n_i the intrinsic carrier concentration.

Considering the E_Y−distribution toward the Schottky contact, in cases of either Y_R=0μm [11]−[12] or very thin Y_R, E_Y increases up to the E_{SCH} value as reported in Fig.2.b. However, if Schottky and p^+−n junctions are far apart each other ($Y_R > X_{CH}/2$) and being unbiased, E_Y can reach a maximum value at $y=-(X_{CH}+Y_G)/2$, similarly to a JFET−structure [15], and then decreases to E_{SCH} with a slope of qN_{EPI}/ε as schematized in Fig.2.c. In order to clarify

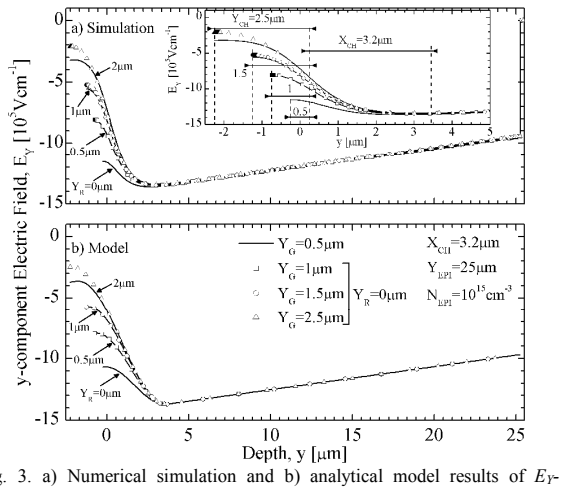

Fig. 3. a) Numerical simulation and b) analytical model results of E_Y-distribution along y-axis for a JBS diode with X_{CH}=3.2μm, Y_{EPI}=25μm, $N_{EPI}=10^{15}cm^{-3}$, V_D=3kV and T=300K. Lines are for Y_G=0.5μm and different Y_R values, whereas symbols are for Y_R=0μm and different Y_G values.

such behavior in Fig. 3.a numerical simulations [17] of E_Y−distribution for JBS structures with X_{CH}=3.2μm, Y_{EPI}=25μm, N_{EPI}=$10^{15} cm^{-3}$ and at reverse diode voltage V_D=3kV are reported with different values of (Y_G,Y_R). In particular, JBS diodes with (Y_G,Y_R)=(0.5μm,0.5μm) and (0.5μm,1μm) have a maximum electric field at the Schottky contact because $Y_R \leq X_{CH}/2$, whereas (0.5μm,2μm)−structure has a maximum at $y=-(X_{CH}+Y_G)/2$ and decreases up to E_{SCH} with a slope of qN_{EPI}/ε, differently from (2.5μm,0μm)−structure that has a lower $|E_{SCH}|$. Furthermore, in all structures E_{V_D} is at $y=X_{CH}+Y_G/2$. It is interesting to note that, for $Y_R \leq X_{CH}/2$, $p-n$ space charge regions extend across the whole n−region up to the Schottky contact, which results in a full depletion similar to the case with Y_R=0μm. In fact, the numerical simulations depicted in Fig.3.a show that E_Y are equal for those structures having the same $Y_{CH}=Y_G+Y_R$, for example (Y_G,Y_R)=(1μm,0μm) and (0.5μm,0.5μm). It means that it is possible to have the same shielding effect of the Schottky contact and, hence, the same reverse current but avoiding the tilted lateral ion−implantation, thus, simplifying the device process fabrication.

By considering the above results, it follows that the dimensioning of the inner part of the channel, which is X_{CH}−width and λ–depth, requires a 2D solution of Poisson's equation:

$$\begin{cases} \nabla^2 \phi(x',y') = -\dfrac{qN_{EPI}}{\varepsilon} \\ \phi(0,\lambda) = \phi^* \\ \left.\dfrac{\partial \phi}{\partial y'}\right|_{(0,\lambda)} = E_{V_D} \end{cases} \tag{4}$$

where all the quantities are reported in Tab. I, $V_{bi} = V_{bi}^{pn} - V_{bi}^{SB}$, $V_{bi}^{SB} = WF - \chi - V_T \ln(N_C/N_{EPI})$ is the Schottky junction built−in voltage, WF the metal work function, χ the semiconductor electron affinity and N_C the effective density of states in the conduction band, whereas, outside this area, an 1D variation of the potential distribution can be assumed. It is worth to note that to simplify the expression of (4) the origin of the axis has been shifted on the position of the maximum E_Y as reported in both JBS cross−sections of Fig.2.b and c. By using the superposition principle, the potential can be written as $\Phi(x',y')=\Phi_L(x',y')+\Phi_P(y')$ where $\Phi_L(x',y')$ can be solved as a Laplace problem and $\Phi_P(y')$ can be reduced to a one-dimensional Poisson problem that takes into account the charge into the channel, whose boundary conditions are reported in Tab. I [18]:

TABLE I
BOUNDARY CONDITIONS

$Y_R \leq \frac{X_{CH}}{2}$	$Y_R > \frac{X_{CH}}{2}$
$Y_1 = 0$	$Y_1 = Y_R - X_{CH}/2$
$\phi_0 = 0$	$\phi_0 = \phi(0^-) = \frac{qN_{EPI}}{2\varepsilon} Y_1^2 + k_3 Y_1$ $\left.\frac{\partial \phi}{\partial y'}\right\|_{y'=0} = k_3$
$\phi^* = X_{CH} \frac{E_{pn} + E_{V_D}}{2} - V_{bi} + \phi_0$	
$\lambda = X_{CH} + Y_G + Y_R - Y_1$	
$\Phi_L(x',0) = \Phi_L(x',\lambda) = 0$ $\left.\frac{\partial \phi_L}{\partial x}\right\|_{x=0} = 0$	
$\Phi_P(0) = 0$	

$$\nabla^2 \phi_L(x',y') = 0 \tag{5.a}$$

$$\nabla^2 \phi_P(y') = -\frac{qN_{EPI}}{\varepsilon} \tag{5.b}$$

Both for $Y_R > X_{CH}/2$ and for $Y_R \leq X_{CH}/2$, the solutions of (5) are as follows:

$$\phi_L(x',y') = k_1 \sin\left(\frac{\pi}{\lambda} y'\right) \cosh\left(\frac{\pi}{\lambda} x'\right) \tag{6.a}$$

$$\phi_P(y') = -\frac{qN_{EPI}}{2\varepsilon} y'^2 + k_2 y' + \phi_0 \tag{6.b}$$

where k_1 and k_2 are reported in Tab. II. From (6) one obtains Φ and E_Y distributions, whose expressions are reported in Tab. II, calculated at x=0 for each region. In Fig.3.b analytical curves of E_Y are shown, derived from the same structures of the simulations in Fig.3.a. The agreement between the curves of the two figures show the correctness of the analytical derivation.

Finally, the electric field at the Schottky contact can be written as follows:

$$|E_{SCH}| = \left| E_{pn} + \frac{qN_{EPI}}{\varepsilon}(Y_G + Y_R - 2Y_1) - 2k_2 \right| \tag{7}$$

which can be used both to design the channel region of JBS diodes and to calculate the diode reverse current as reported in the next section. It is worth to note that for the generality of the above equations, the derived model can be applied to any JBS geometry, without particular limitations.

TABLE II
SOLUTIONS OF (4) FOR x=0

y'	$[-Y_1;0]$	$[0;\lambda]$	$[\lambda;Y_{EPI}+\lambda]$
$Y_R \leq \frac{X_{CH}}{2}$	$\phi = 0$ $E_Y = 0$	$\phi = k_1 \sin\left(\frac{\pi}{\lambda} y'\right) - \frac{qN_{EPI}}{2\varepsilon} y'^2 + k_2 y' + \phi_0$ $E_Y = -k_1 \frac{\pi}{\lambda} \cos\left(\frac{\pi}{\lambda} y'\right) + \frac{qN_{EPI}}{\varepsilon} y' - k_2$	$\phi = -\frac{qN_{EPI}}{2\varepsilon}(y'-\lambda)^2 + E_{V_D}(y'-\lambda) + \phi^*$ $E_Y = \frac{qN_{EPI}}{\varepsilon}(y'-\lambda) - E_{V_D}$
$Y_R > \frac{X_{CH}}{2}$	$\phi = -\frac{qN_{EPI}}{2\varepsilon}(y'^2 - Y_1^2) + \left(\frac{\pi}{\lambda} k_1 + k_2\right)(y' + Y_1)$ $E_Y = \frac{qN_{EPI}}{\varepsilon} y' + \left(\frac{\pi}{\lambda} k_1 + k_2\right)$		

$$k_1 = \frac{\lambda}{\pi}\left(-E_{V_D} - \frac{qN_{EPI}}{\varepsilon}\lambda + k_2\right) \qquad k_2 = \frac{1}{\lambda}\left[E_{pn} X_{CH} + \frac{qN_{EPI}}{2\varepsilon}\left(\lambda^2 - X_{CH}^2\right) - V_{bi}\right]$$

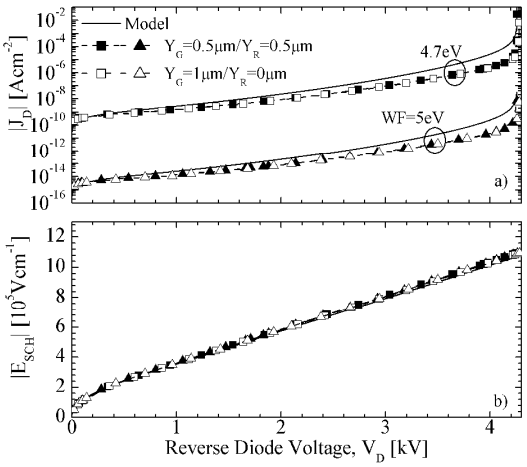

Fig. 4. Comparisons between model and numerical simulation of a) J_D-V_D and b) E_{SCH}–V_D for the structure in Fig. 2.a with $X_{CH}=3.2\mu m$, $Y_{EPI}=25\mu m$, $N_{EPI}=10^{15}cm^{-3}$ and $T=300K$.

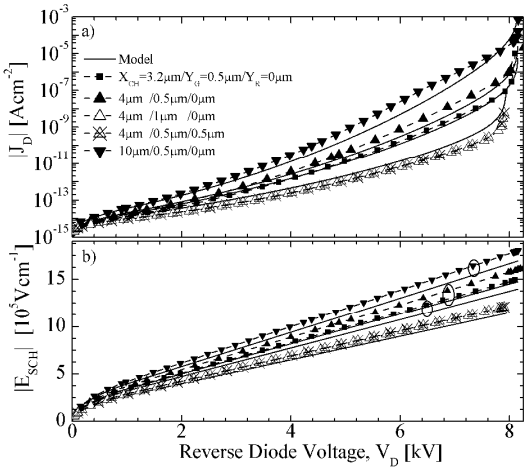

Fig. 5. Comparisons between model and numerical simulation of a) J_D–V_D and b) E_{SCH}–V_D for the structure in Fig.2.a with $Y_{EPI}=50\mu m$, $WF=5eV$, $N_{EPI}=5\cdot10^{14}cm^{-3}$ and $T=300K$.

IV. Model Validations

To validate the model we report comparisons with E_{SCH}–V_D and J_D–V_D curves obtained with numerical simulations [17] as well as with diode reverse characteristics of experimental diodes having different X_{CH}.

A. Numerical simulations

Using the thermionic-field emissions model for 4H-SiC JBS devices [14], the reverse diode current depends on E_{SCH}, which is given from (7) as follows [19]:

$$I_{TFE} = ZX_{CH}A_{TE}E_{SCH}e^{-\frac{\phi_B}{V_T}+B_{TE}E_{SCH}^2} \tag{8}$$

where $A_{TE} = 10^2\frac{A^*Tqh}{k}\sqrt{\frac{1}{kT8\pi m^*}}$, $B_{TE} = \frac{10^4(qh)^2}{(kT)^3\,96\pi^2 m^*}$, Z is the device length, $A^*=146AK^{-2}cm^{-2}$ Richardson's constant, T the device temperature, V_T the thermal voltage, Φ_B the barrier height, q the electron charge, ε the semiconductor dielectric permittivity, m^* the semiconductor effective mass, and h Plank constant. Then, by taking into account the avalanche current, J_D can be modeled with the well known equation [10]–[12]:

$$J_D = M\left[\frac{I_{TFE}}{Z(X_{CH}+X_G)}+J_{GR}\right] \tag{9}$$

where $M=(1-(V_D/BD)^{\alpha})^{-1}$ is the avalanche multiplication coefficient, J_{GR} generation–recombination p–n reverse current [20], BD the breakdown voltage, and X_G the p–region width.

In this analysis, JBS structures have different values of epilayer doping and thickness, of channel width and depth and of metal work function. Physical models include field dependent and carrier mobility, SRH recombination, incomplete ionization, bandgap narrowing and avalanche multiplication, whose parameters are in [16],[21]. For the tunnelling parameters we have $A_{TE}=2\cdot10^2Acm^{-1}V^{-1}$ and $B_{TE}=6.13\cdot10^{-12}cm^2V^{-2}$ for which we used $m^*=0.3m_0$ [11].

In Fig.4 J_D and E_{SCH} as V_D–function are reported for JBS structures with $X_{CH}=3.2\mu m$, $Y_{EPI}=25\mu m$ and $N_{EPI}=10^{15}cm^{-3}$ and with different values of WF and (Y_G,Y_R). By observing Fig.4.b although two different couples of (Y_G,Y_R) are used, i.e. $(0.5\mu m,0.5\mu m)$ and $(1\mu m,0\mu m)$, E_{SCH}–V_D curves are equal. In fact, being Y_R less than $X_{CH}/2=1.6\mu m$, the whole channel is fully depleted and E_Y along y–axis is equal as reported in Fig.3. Electrical characteristics have similar behaviors, just only a shift towards higher current by reducing qWF from $5eV$ to $4.7eV$, which is due to the reduction of the barrier height $q\Phi_{B0}$ from $1.3eV$ to $1eV$. In all structures J_D is mainly due to the thermionic emission, I_{TE}, as also shown by low E_{SCH} values ($<1MV/cm$); the further increase of J_D is due to the avalanche breakdown of the p–i–n diode ($V_{BD}^{pn}=4.3kV$).

In Fig. 5 J_D–V_D and E_{SCH}–V_D curves of JBS diodes with $qWF=5eV$, $Y_{EPI}=50\mu m$ and $N_{EPI}=5\cdot10^{14}cm^{-3}$ are compared by changing X_{CH}, Y_G and Y_R values. It is clear that E_{SCH} increases as well as J_D either widening or thinning the channel region. In particular, for $Y_G=0.5\mu m$ and $Y_R=0\mu m$, the weak shielding effect of p–regions causes an increase of E_{SCH} over $1MV/cm$ and, as consequence, the tunneling mechanism, I_{FE}, prevails on the thermionic one and, comparing JBS with $X_{CH}=3.2\mu m$ and $10\mu m$, J_D increases by five order of magnitude at the same diode voltage and before the avalanche breakdown. Moreover, also in this case, JBS diodes with the same Y_{CH}, i.e. $(Y_G,Y_R)=(0.5\mu m,0.5\mu m)$ and $(1\mu m,0\mu m)$, and having $Y_R<X_{CH}/2$ show the same reverse behavior both for J_D and for E_{SCH}.

In Fig. 6 R_D–V_{BL} curves are reported for $N_{EPI}=10^{15}cm^{-3}$, $Y_{EPI}=25\mu m$ and various Y_{CH} values, which are obtained from (1) and from the following equation for $Y_{CH}\leq Y_G+X_{CH}/2$ using (3):

$$V_{BL} = V_{PT} + Y_{EPI}E_{pn} - q\frac{N_{EPI}}{\varepsilon}Y_{EPI}^2 \tag{10}$$

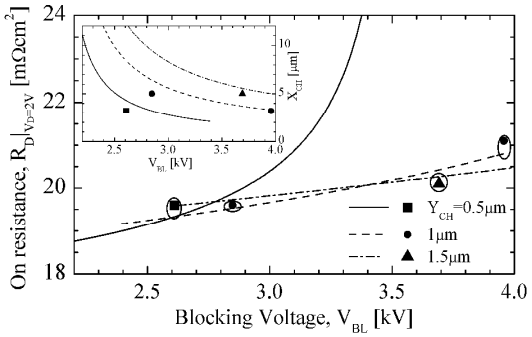

Fig. 6. R_D-V_{BL} curves for different Y_{CH} values obtained for $I_{TE}/I_{FE}=100$ ($|E_{SCH}|=1MVcm^{-1}$), $N_{EPI}=10^{15}cm^{-3}$ and $Y_{EPI}=25\mu m$. In the insert the respective X_{CH}–V_{BL} curves are shown. Numerical simulation data are in symbols.

where $E_{pn}=\dfrac{\lambda E_{SCH}+2V_{bi}+qN_{EPI}\varepsilon^{-1}\left(\lambda X_{CH}+X_{CH}^2-\lambda^2\right)}{2X_{CH}-\lambda}$ is from (7) substituting k_2 of Tab. II. Comparing the results for $Y_{CH}=0.5\mu m$ and $1.5\mu m$, it is evident that for thinner channels a significant variation of R_D is shown for small variation of V_{BL}, differently from deeper channels where R_D almost remains constant, because of its less dependence on X_{CH}. However, for all cases a wider channel causes a larger variation of V_{BL} as reported in the insert of Fig. 6. In both graphs, model results are also compared with simulation data (symbols).

B. Experimental comparison

Experimental JBS diodes are fabricated with two channel geometries (X_{CH},X_G)=($4.5\mu m$,$3\mu m$) and ($3\mu m$,$4.5\mu m$), respectively, for JBS#1 and JBS#2. Both have titanium as Schottky metal contact, $N_{EPI}=9.1\cdot10^{15}cm^{-3}$, $Y_{EPI}=12.2\mu m$, a contact area of $9.46\cdot10^{-3}cm^2$, planar p-regions ($Y_R=0\mu m$) with $Y_G=0.4\mu m$. On the same wafer Schottky diodes are also fabricated and from forward curves we extracted $\Phi_{B0}=1.04eV$ and $R_D=6.6m\Omega cm^2$ and from reverse characteristics $A_{TE}=1.09\cdot10^2Acm^{-1}V^{-1}$ and $B_{TE}=1.83\cdot10^{-12}cm^2V^{-2}$. These parameters are needed in order to tune Schottky junction parameters, i.e. Φ_{B0}, A_{TE} and B_{TE}, which depend on the device fabrication process. Once such parameters are defined, we only change the channel geometry (X_{CH},X_G) in accord with the experimental data.

In Fig. 7 J_D–V_D reverse characteristics from the model accurately describe the behaviour of the experimental data.

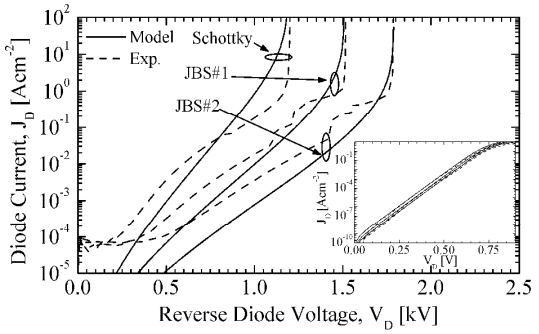

Fig. 7. Comparisons between model and measurements of reverse J_D–V_D characteristics for the structure in Fig. 2.a with $Y_G=0.4\mu m$, $Y_R=0\mu m$, $Y_{EPI}=12.2\mu m$, $N_{EPI}=9.1\cdot10^{15}cm^{-3}$, $\Phi_{B0}=1.04eV$ and $T=300K$. In the insert $ln(J_D)$–V_D forward curves.

Although the tunnelling current through the Schottky barrier is shown in all devices, JBS#2 diode is less dependent on the reverse voltage due to the more efficient shielding effect of p–regions. If, on the one hand, a low X_{CH} value improves the reverse behaviour, on the other hand, it increases the forward voltage drop due to the channel and spreading components of the diode resistance in (1). In fact, R_D increases to $6.9m\Omega cm^2$ and $7.1m\Omega cm^2$, respectively, for $X_{CH}=4.5\mu m$ and $3\mu m$. This result is also predicted by the model: when the blocking voltage, V_{BL}, is defined as the voltage for which $E_{SCH}=1.95MVcm^{-1}$, from (1) and (10) one obtains ($1.56kV$,$7m\Omega cm^2$) and ($1.8kV$,$7.1m\Omega cm^2$) respect to experimental data ($1.51kV$,$6.9m\Omega cm^2$) and ($1.78kV$, $7.3m\Omega cm^2$) for JBS#1 and JBS#2, respectively. It is worth to note that at $E_{SCH}=1.95MVcm^{-1}$ one obtains the breakdown both of Schottky and of p^+–n junctions.

V. Model Implementation for JBS Design

Although the model can also describe the reverse characteristics of JBS diodes, we use it as a first-order tool for the design of JBS diodes. In order to achieve this aim, we need to express the channel parameters (X_{CH},Y_{CH}) in terms of (R_D,V_{BL}) for a given values of N_{EPI}, Y_{EPI} and E_{SCH}. Let us consider a device structure as in Fig.2.b ($Y_{CH}\le Y_G+X_{CH}/2$) and, by manipulating (2), (3) and (7), the couple (X_{CH},Y_{CH}) can be calculated as follows:

$$X_{CH1,2}=\frac{-b\pm\sqrt{b^2-4ac}}{2a} \tag{11}$$

and

$$Y_{CH1,2}=\frac{1}{\rho_{EPI}}\frac{X_{CH}}{X_{CH}+X_G}R-\frac{X_G}{2} \tag{12}$$

where $a=E_{pn}-E_{SCH}+qN_{EPI}\varepsilon^{-1}\left(R\rho_{EPI}^{-1}-0.5X_G\right)$,

$b=X_G\left(E_{pn}-E_{SCH}\right)-2V_{bi}+$

$+\left(\dfrac{X_G}{2}-\dfrac{R}{\rho_{EPI}}\right)\left(E_{pn}+E_{SCH}\right)-\dfrac{qN_{EPI}}{\varepsilon}\dfrac{X_G^2}{2}$,

$c=-2V_{bi}X_G+\left(E_{pn}+E_{SCH}\right)0.5X_G^2$, E_{pn} is from (3) with $V_D=V_{BL}$, $R\approx R_D-R_{EPI}-R_{SUB}-R_{CONT}$ and E_{SCH} depends on definition of V_{BL}. In Fig.8 a process flow to design JBS diodes is reported where V_{BD}^{pn} is the breakdown voltage for the p–i–n diode.

For example, we have to design a JBS diode with $N_{EPI}=10^{15}cm^{-3}$ and $Y_{EPI}=25\mu m$ able to manage a $V_{BL}=4kV$ with $R_D=18.5m\Omega cm^2$. One obtains ($3.45\mu m$,$0.98\mu m$) from (11)-(12) and (X_{CH},Y_{CH})=($3.27\mu m$,$1\mu m$) from (1) and (10), which is also reported in Fig. 6, whereas numerical simulation gives (V_{BL},R_D)=($3.96kV$,$21.1m\Omega cm^2$) for (X_{CH},Y_{CH})=($3.2\mu m$,$1\mu m$).

It is worth to note that the slightly difference between the two model results is due to have considered $R_{CH}+R_{SP}=\rho_{EPI}\left(Y_{CH}+0.5X_G\right)\left(X_{CH}+X_G\right)X_{CH}^{-1}$ for (11)-(12) which has been necessary to avoid transcendental equation. Making this assumption means that there is not a

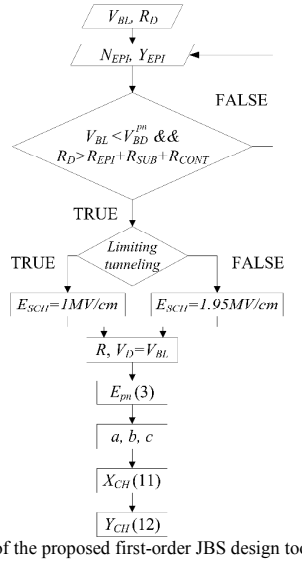

Fig. 8. Flow chart of the proposed first-order JBS design tool.

current spreading outside the channel and $R_{CH} + R_{SP}$ is the highest possible resistance, which can be considered as the worst case.

VI. Conclusion

An analytical instrument to design JBS diodes is reported, based on a physical model of the device. The model calculates the Schottky electric field in terms of geometrical, physical and electrical quantities and works for planar and trenched JBS structures.

In terms of the electrical performances, it can be used to describe the reverse J_D-V_D curves and we have shown its accuracy from comparisons both with experimental data and with numerical simulations changing different device structures. The model can be a starting point to make a compact model for circuit simulator.

Furthermore, an explicit expression of the channel geometry in terms of on-series resistance and blocking voltage has been obtained. Such result has been used as a first-order tool to begin the design process of the channel region. The compactness of the derived expressions, allows one to easily extend the model to all the devices with a similar vertical structure and, in particular, with an intrinsic JFET region, i.e. a horizontal *p-n-p* junctions, by an appropriate adaptation of the boundary conditions to solve a specific Poisson's problem.

References

[1] R.J. Callanan, A. Agarwal, A. Burk, M. Das, B. Hull, F. Husna, A. Powell, J. Richmond, S.H. Ryu, Q.Zhang, "Recent progress in SiC DMOSFETs and JBS diodes at Cree," *IEEE 2008 Annual Conference on Industrial Electronics*, pp.2885-2890, Nov. 2008.

[2] V. Scarpa, U. Kirchner, R. Kern, and R. Gerlach, "New SiC thin-wafer technology paving the way of Schottky diodes with improved performance and reliability," Power Electron. Eur., no. 3, pp. 30–32, 2012.

[3] M. Draghici, R. Rupp, R. Gerlach,and B. Zippelius, "A new 1200V SiC MPS diode with improved performance and ruggedness", *Mat. Sc. For.*, vol. 821−823, pp. 608−611, 2015.

[4] K. Konishi, N. Kameshiro, N. Yokoyama, A. Shima, and Y. Shimamoto, "Influence of trench structure on reverse characteristics of 4H−SiC JBS diodes", *Mat. Sc. For.*, vol. 821−823, pp. 596−599, 2015.

[5] T. Nakamura Y. Nakano, M. Aketa, R. Nakamura, S. Mitani, H. Sakairi, and Y. Yokotsuji, "High performance SiC trench devices with ultra−low ron", *Proc. IEEE Int. Electr. Dev. Meeting*, pp. 26.5.1–26.5.3, Dec. 2011.

[6] N. Ren, J. Wang, and K. Sheng, "Design and experimental study of 4H−SiC trenched junction barrier Schottky diode" *IEEE Trans. Electr. Dev.*, vol. TED−61, no. 7, pp. 2459–2465, Jul. 2014.

[7] B.A. Hull, J.J. Sumakeris, M.J. O'Loughlin, Q. Zhang, J. Richmond, A.R. Powell, E.A. Imhoff, K.D. Hobart, A. Rivera−López, and A.R. Hefner, "Performance and stability of large area 4H−SiC 10kV junction barrier Schottky rectifiers" *IEEE Trans. Electr. Dev.*, vol. TED−55, no. 8, pp. 1864–1870, Aug. 2008.

[8] H. Okino, N. Kameshiro, K. Konishi, N. Inada, K. Mochizuki, A. Shima, N. Yokoyama, and R. Yamada, "Electrical Characteristics of Large Chip-size 3.3kV SiC-JBS diodes", *Mat. Sc. For.*, vol. 740−742, pp. 881−886, 2013.

[9] K. Asano, T. Hayashi, R. Saito, and Y. Sugawara, "High Temperature Static and Dynamic Characteristics of 3.7kV High Voltage 4H-Sic JBS" *Power Semicond. Devices and ICs (ISPSD)* 2000, pp.97-100, May 2010.

[10] L. Zhu, and T.P. Chow, "Analytical modeling of high−Voltage 4H−SiC junction barrier Schottky (JBS) rectifiers" *IEEE Trans. Electr. Dev.*, vol. TED−55, no. 8, pp. 1857–1863, Aug. 2008.

[11] R. Radhakrishnan, and J.H. Zhao,"A 2−dimensional fully analytical model for design of high voltage junction barrier Schottky (JBS) diodes" *Solid State Electron.*, vol. 63, pp. 167–176, 2011.

[12] N. Ren, and K. Sheng, "An analytical model with 2−D effects for 4H−SiC trenched junction barrier Schottky diodes" *IEEE Trans. Electr. Dev.*, vol. TED−61, no. 12, pp. 4158–4165, Dec. 2014.

[13] L. Di Benedetto, S. Bellone, R. Nipoti and G.D. Licciardo, "On the crossing−point of 4H−SiC power diodes characteristics" *IEEE Electr. Dev. Lett.*, vol. EDL−35, no. 2, pp. 244–246, Feb. 2014.

[14] T. Kimoto and J. A. Cooper, *Fundamentals of Silicon Carbide Technology: Growth, Characterization, Devices, and Applications*, 1st ed. Singapore: John Wiley & Sons, 2014.

[15] S. Bellone and L. Di Benedetto, "A model of the J_D−V_{GS} characteristics of normally−off 4H−SiC bipolar JFETs," *IEEE Trans. Power Electron.,* vol. PEL–29, no. 1, pp. 514–521, Jan. 2014.

[16] S. Bellone, L. Di Benedetto, and G.D. Licciardo, "A model of the off−behaviour of 4H−SiC power JFETs" *Solid State Electron.*, vol.109, pp.17–24, Jul. 2015.

[17] SILVACO Int., Santa Clara, CA, ATLAS User's Manual, 2005, Ver. 5.10R.

[18] C. Bulucea and A. Rusu, "A first−order theory of the static induction transistor," *Solid State Electron.*, vol. 30, no. 12, pp. 1227–1242, 1987.

[19] T. Hatakeyama and T. Shinohe, "Reverse characteristics of a 4H-SiC Schottky barrier diode," *Mater. Sci. For.*, vol. 389-393, pp. 1169–1172, 2002.

[20] B. J. Baliga, *Fundamentals of Power Semiconductor Devices*, 1st ed. New York: Springer−Verlag, 2008.

[21] S. Bellone and L. Di Benedetto, "Design and Performances of 4H−SiC Bipolar Mode Field Effect Transistor (BMFETs)", *IEEE Trans. on Power Electron*., vol.29, no.5, pp. 2174−2179, May 2014.